Research Article | Vol. 8, No. 2 | 1 Feb 2017 | BIOMEDICAL OPTICS EXPRESS 736

Biomedical Optics EXPRESS

In vivo photoacoustic lipid imaging in mice using the second near-infrared window

GURNEET S. SANGHA,[1] EVAN H. PHILLIPS,[1] AND CRAIG J. GOERGEN[1,2,*]

[1]*Weldon School of Biomedical Engineering, Purdue University, 206 S. Martin Jischke Dr., West Lafayette, IN 47907, USA*
[2]*Purdue University Center for Cancer Research, Purdue University, 201 S. University St., West Lafayette, IN 46907, USA*
[*]*cgoergen@purdue.edu*

Abstract: Photoacoustic imaging has emerged as a promising technique to improve preclinical and clinical imaging by providing users with label-free optical contrast of tissue. Here, we present a proof-of-concept study for noninvasive *in vivo* murine lipid imaging using 1210 nm light to investigate differences in periaortic fat among mice of different gender, genotypes, and maturation. Acquired lipid signals suggest that adult male apoE$^{-/-}$ mice have greater periaortic fat accumulation compared to adolescent males, apoE$^{-/-}$ females, and wild-type mice. These results demonstrate the potential of photoacoustic tomography for studying vascular pathophysiology and improving the diagnosis of lipid-based diseases.

OCIS codes: (110.0110) Imaging systems; (110.5120) Photoacoustic imaging.

References and links

1. G. Vernon, A. Baranova, and Z. M. Younossi, "Systematic review: the epidemiology and natural history of non-alcoholic fatty liver disease and non-alcoholic steatohepatitis in adults," Aliment. Pharmacol. Ther. **34**(3), 274–285 (2011).
2. A. J. Lucas, "Atherosclerosis," Nature **407**, 233–241 (2000).
3. K. M. Flegal, M. D. Carroll, C. L. Ogden, and L. R. Curtin, "Prevalence and trends in obesity among US adults, 1999-2008," JAMA **303**(3), 235–241 (2010).
4. G. S. Sangha and C. J. Goergen, "Photoacoustic tomography: applications for atherosclerosis imaging," J. Opt. **18**(8), 084005 (2016).
5. H.-W. Wang, N. Chai, P. Wang, S. Hu, W. Dou, D. Umulis, L. V. Wang, M. Sturek, R. Lucht, and J.-X. Cheng, "Label-free bond-selective imaging by listening to vibrationally excited molecules," Phys. Rev. Lett. **106**(23), 238106 (2011).
6. T. J. Allen, A. Hall, A. P. Dhillon, J. S. Owen, and P. C. Beard, "Spectroscopic photoacoustic imaging of lipid-rich plaques in the human aorta in the 740 to 1400 nm wavelength range," J. Biomed. Opt. **17**(6), 061209 (2012).
7. R. Li, E. Phillips, P. Wang, C. J. Goergen, and J. X. Cheng, "Label-free in vivo imaging of peripheral nerve by multispectral photoacoustic tomography," J. Biophotonics **9**(1-2), 124–128 (2016).
8. P. Iozzo, "Myocardial, perivascular, and epicardial fat," Diabetes Care **34**(Suppl 2), S371–S379 (2011).
9. K. Flurkey, J. M. Currer, and D. E. Harrison, "Mouse models in aging research," in *The Mouse in Biomedical Research* (Elsevier, 2007).
10. F. W. Damen, A. R. Adelsperger, K. E. Wilson, and C. J. Goergen, "Comparison of traditional and integrated digital anesthetic vaporizers," J. Am. Assoc. Lab. Anim. Sci. **54**(6), 756–762 (2015).
11. Y. Nakashima, A. S. Plump, E. W. Raines, J. L. Breslow, and R. Ross, "ApoE-deficient mice develop lesions of all phases of atherosclerosis throughout the arterial tree," Arterioscler. Thromb. **14**(1), 133–140 (1994).
12. C. M. Alvarado, J. A. Diaz, A. E. Hawley, S. K. Wrobleski, R. E. Sigler, and D. D. Myers, Jr., "Male mice have increased thrombotic potential: sex differences in a mouse model of venous thrombosis," Thromb. Res. **127**(5), 478–486 (2011).
13. C. J. Goergen, K. N. Barr, D. T. Huynh, J. R. Eastham-Anderson, G. Choi, M. Hedehus, R. L. Dalman, A. J. Connolly, C. A. Taylor, P. S. Tsao, and J. M. Greve, "In vivo quantification of murine aortic cyclic strain, motion, and curvature: implications for abdominal aortic aneurysm growth," J. Magn. Reson. Imaging **32**(4), 847–858 (2010).
14. C. J. Goergen, J. Azuma, K. N. Barr, L. Magdefessel, D. Y. Kallop, A. Gogineni, A. Grewall, R. M. Weimer, A. J. Connolly, R. L. Dalman, C. A. Taylor, P. S. Tsao, and J. M. Greve, "Influences of aortic motion and curvature on vessel expansion in murine experimental aneurysms," Arterioscler. Thromb. Vasc. Biol. **31**(2), 270–279 (2011).

#275724 http://dx.doi.org/10.1364/BOE.8.000736
Journal © 2017 Received 3 Oct 2016; revised 9 Dec 2016; accepted 23 Dec 2016; published 10 Jan 2017

Biomedical Optics EXPRESS

15. E. H. Phillips, A. A. Yrineo, H. D. Schroeder, K. E. Wilson, J.-X. Cheng, and C. J. Goergen, "Morphological and biomechanical differences in the elastase and AngII apoE rodent models of abdominal aortic aneurysms," BioMed research international **2015**, 1–12 (2015).

1. Introduction

Lipid-based diseases account for a significant portion of Western world mortality [1–3]. Clinical manifestations of lipid-based conditions appear in a multitude of debilitating disease states that include diabetes, obesity, fatty liver disease, demyelination, and vascular diseases such as coronary artery disease and peripheral artery disease. As a result, many imaging techniques including ultrasonography, magnetic resonance imaging, positron emission tomography, x-ray angiography, and optical imaging have been developed to better characterize these conditions. While these imaging modalities can be effective in studying a wide variety of disease states, each has its own inherent limitations such as high cost, limited penetration depth, and/or long imaging times [4]. Therefore, there is still a need to develop techniques that can better characterize compositional information in a rapid, label-free, noninvasive manner that complements currently used imaging methods.

Photoacoustic tomography (PAT) is an emerging modality that can improve *in vivo* disease characterization in humans and animals [4,5]. Compared to traditional photoacoustic techniques, PAT, using the second near-infrared window, provides optical-dependent contrast that allows users to differentiate biological components such as blood and fat [6,7]. This contrast is produced by using pulsed laser light to induce a transient temperature rise in tissue that causes acoustic wave propagation. These acoustic waves are acquired to reconstruct an image that displays the relative density and location of biological components. PAT also allows the user to tune the wavelength of light to monitor the excitation of distinct molecular overtones. For instance, the second overtone vibrations of the CH_2 bonds can be detected by using 1210 nm light to identify lipid deposition [4]. When overlaid with ultrasound images, we obtain anatomical and compositional information that other modalities cannot easily provide. In fact, previous *ex vivo* and intravascular studies have shown that PAT can identify mild fatty streaks and discriminate between fibrous and lipid-rich plaques [5]. Despite the exciting potential of PAT, its use in noninvasive *in vivo* imaging of lipid-based murine disease models to better understand disease initiation and progression has not been explored.

Here we present our findings on how PAT can be utilized to study lipid accumulation in hyperlipidemic mice. We focused on the periaortic fat in mice, as it is ample, metabolically active, and accumulates throughout the vasculature. Studying excessive periaortic fat may also have clinical implication as it is involved in cardiovascular and metabolic dysfunction [8]. We hypothesized that PAT can be utilized to image and detect significant differences in lipid accumulation between apolipoprotein E-deficient ($apoE^{-/-}$) and wild-type (WT) mice. The methods and results in this paper are significant as this is the first report to our knowledge that utilizes long wavelength PAT for noninvasive *in vivo* lipid detection in mice.

2. Materials and methods

$ApoE^{-/-}$ (n = 17) and WT (n = 10) mice were obtained from Jackson Laboratory (Bar Harbor, ME) and fed a standard chow diet. These mice were separated into six distinct groups based on gender and maturation as shown in Table 1 [9]. A small animal anesthesia system (SomnoSuite, Kent Scientific [10]) was used to keep the mouse under anesthesia using 1.5-3% isoflurane and 225 mL/min room air. Prior to imaging, eye lubricant was applied to each animal to prevent corneal desiccation. We kept rectal temperature at roughly 34-36°C with a heated stage and monitored this using a rectal probe. Furthermore, heart rate was maintained between 450 and 600 beats per minute while respiration rate was kept between 40 and 80 breaths per minute and monitored using electrodes built into the heated stage.

Biomedical Optics EXPRESS

Table 1. Summary of the Characteristics for Experimental Mouse Groups

Genotype	apoE−/−				WT	
Gender	Male		Female		Male	
Maturation	Adolescent	Adult	Adolescent	Adult	Adolescent	Adult
n	5	4	4	4	5	5
Age (months)	2.96 ± 0	11.7 ± 2.7	2.69 ± 0.2	9.40 ± 0	2.79 ± 0	5.99 ± 0.20
Weight (g)	30.3 ± 1.0	32.2 ± 2.1	23.8 ± 2.5	32.8 ± 3.9	26.3 ± 2.9	32.8 ± 4.7

We used a high-frequency small animal ultrasound system (Vevo2100, FUJIFILM Visual Sonics) equipped with a 40 MHz center frequency transducer (MS550D) to obtain *in vivo* long-axis B-mode and PAT images of the infrarenal aorta. A Nd:YAG pulsed optical parametric oscillator (OPO) laser (NT352C, Ekspla) capable of producing 670 to 2300 nm light was used to generate 5 ns pulses at 10 Hz. Our system design has been previously summarized [7] and has been recapitulated in Fig. 1. A function generator (4013B, B&K Precision) was used to synchronize pulse excitation and image acquisition between the laser and the ultrasound, and a pulse generator (9200, Quantum Composers) was used to coordinate the trigger of the laser with the ultrasound system. The function generator specifically produced a 10 Hz, 5 V square waveform. This setup provided us an ultrasound axial spatial resolution of 40 μm with pixel size of 13.2x55.0 μm (axial x lateral), and PAT axial spatial resolution of 124 μm with pixel size of 28.4x26.6 μm [7].

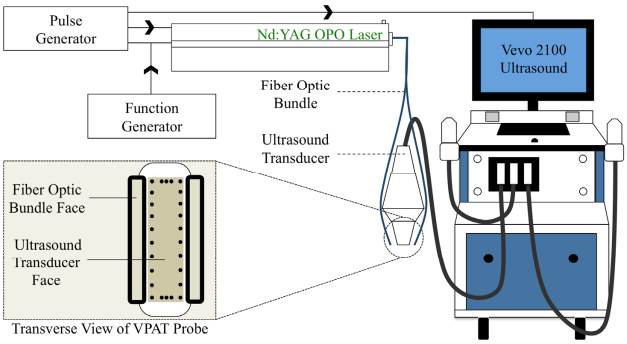

Fig. 1. Schematic depicting PAT setup. Nd:YAG OPO laser delivered light through a fiber optic bundle to an anesthetized mouse. A 40 MHz center frequency transducer was used to acquire the resulting PAT signal. A function generator coordinated pulse excitation and image acquisition between the laser and the Vevo2100 ultrasound system. A pulse generator was used to synchronize the trigger of the laser with the ultrasound system. The ultrasound transducer face is 20x5 mm and fiber optic bundle face is 12x2 mm.

In this study, 1210 nm light was used to detect periaortic fat signal along the anterior wall of the infrarenal aorta (Fig. 2 [6]) of apoE$^{-/-}$ and WT mice (Table 1). We used 1100 nm light to detect blood signal [7] within the lumen of the aorta and 1250 nm light as a negative off-resonance control [6]. Photoacoustic images were acquired with a priority of 80%, gain of 30 dB, power of 100%, brightness of 50, and contrast of 50 in the Vevo2100 system. Priority was decreased to 80% to shift the image intensity histogram leftward by 20%. This eliminated many of the background pixels and provided us with better lipid contrast. We chose to remove 20% as it ensured that no part of the histogram was truncated. To minimize minor PAT signal fluctuations and background noise we acquired ten PAT images for each wavelength and computed the pixel-wise arithmetic mean (Fig. 3(A)). We then performed a thresholding technique to discriminate lipid and background signal. A new histogram of each image was obtained, which produced two peaks that represented the background and lipid signal (Fig. 3(B)). A threshold point, in the trough of these two peaks, was chosen to assign pixels a value of 255 if their value was greater than or equal to that of the threshold and assigned 0 otherwise. This PAT mask was overlaid on a grayscale PAT image to confirm the accuracy of our thresholding technique (Fig. 3(C)). If the mask did not properly align on the

Biomedical Optics EXPRESS

grayscale PAT image, the threshold was either increased or decreased by a value of 10 until the mask aligned with the grayscale image. We then plotted the profile of pixel intensities along multiple lines of interest extending anterior to posterior (Fig. 3(D)). The width of the periaortic fat peak was measured to quantify lipid accumulation on the aorta (Fig. 3(E)). This thresholding method was repeated 10 times for each mouse (270 total measurements) to take into account measurement variability. Oil Red O (ORO) lipophilic staining was performed to confirm presence of periaortic fat on an excised mouse aorta. Finally, an ANOVA with a Tukey post-hoc statistical test was used to determine significance between groups ($p<0.05$).

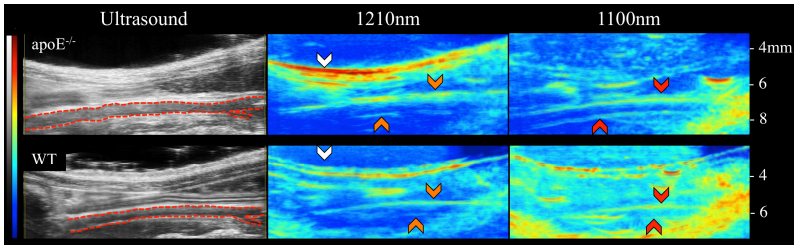

Fig. 2. Ultrasound (left), lipid PAT (middle), and blood PAT (right) images of adult male apoE$^{-/-}$ (top) and WT (bottom) mice. Images are shown such that the animals are orientated in supine position with the head located to the left and tail is located to the right. Greater periaortic fat signal is evident in the apoE$^{-/-}$ mouse compared to the WT mouse. Using these images we can clearly discriminate the infrarenal aorta (red dotted outline), subcutaneous fat (white arrows), periaortic fat (orange arrows), and blood (red arrows).

3. Results

Using our PAT setup we were able to resolve subcutaneous and periaortic fat buildup in both apoE$^{-/-}$ and WT mice. We clearly observed lipid specific PAT signal that followed both the geometry of the skin due to the subcutaneous fat and infrarenal aorta due to periaortic fat accumulation. The adult male apoE$^{-/-}$ mice also showed more subcutaneous and periaortic fat accumulation compared to the adult male WT mice (Fig. 2). To confirm that our lipid signal is coming from periaortic fat, we performed ORO staining on excised aortae of apoE$^{-/-}$ mice. We observed that the entire vessel stained red, confirming the presence of periaortic fat (Fig. 3(F)). This suggests that our lipid signal is indeed coming from fat buildup on top of the vessel. All vessels that underwent this ORO process stained red, making it challenging to detect differences in periaortic fat between mice, thus highlighting the benefits of PAT.

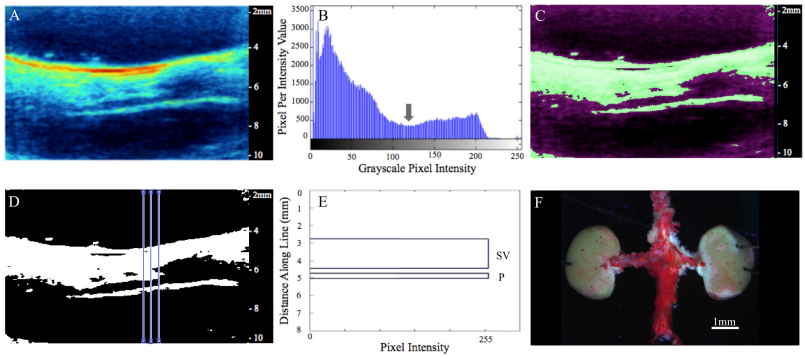

Fig. 3. Averaged PAT image (1210 nm) reveals subcutaneous and periaortic fat (A). Histogram of PAT pixel intensities shows peaks for background and lipid signal (B). Gray arrow represents threshold point used to create PAT mask, which is overlaid on the original PAT image to confirm thresholding accuracy (C). Plot profile analysis was used to measure periaortic thickness at multiple locations (D). Width of top peak (SV) represents subcutaneous and visceral fat and width of bottom peak (P) represents periaortic fat from one plot profile measurement (E). ORO staining on excised aorta confirms periaortic fat accumulation (F).

Biomedical Optics EXPRESS

Prior to quantifying periaortic fat accumulation, we validated our analysis technique to ensure accurate quantification of lipid signal. First, we confirmed that our thresholding technique provides reliable measurements by measuring the inner diameter of polyethylene 50 (PE50) tubing. This was accomplished by acquiring 1100 nm PAT images of a murine blood filled PE50 tube. The thickness of the blood signal was measured at three locations along the tube and compared to the known inner diameter (0.58 mm). Using our threshold algorithm we obtained an experimental inner diameter of 0.553 ± 0.012 mm, resulting in a percent error of 4.7%. This variation is possibly due to differences in acoustic speeds through water and PE50 tubing. We also showed that there is no measurement variation due to respiratory or cardiac motion by quantifying lipid thickness in both the raw PAT and the pixel-wise arithmetic mean images. To prevent measurement bias we quantified thickness at the same location throughout the aorta (Fig. 4). Our analysis showed respiratory and cardiac motion does not affect our results, as there are no statistically significant differences in fat thickness between the raw and mean images ($p>0.05$). Furthermore, we observed greater lipid signal towards the surface of the mouse due to progressively fewer photons reaching deeper structures. To overcome this limitation we used lipid thickness as our quantification marker rather than signal intensity.

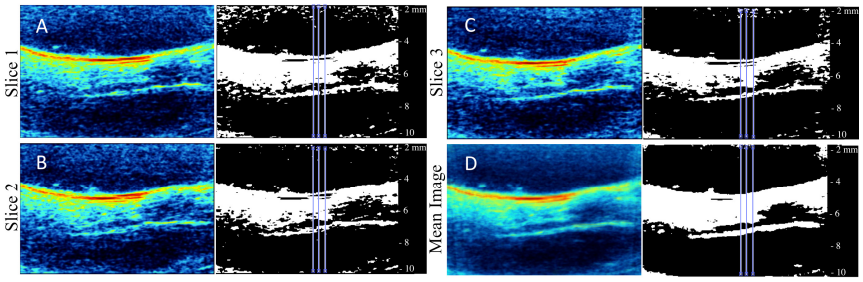

Fig. 4. Three representative raw 1210 nm PAT and measurement images (A-C) and mean (D) image of an apoE$^{-/-}$ mouse. Measurements were taken in same location in all images.

We then used our thresholding technique to quantify lipid thickness in adolescent male (0.24 ± 0.06 mm), adult male (0.46 ± 0.12 mm), adolescent female (0.24 ± 0.08 mm), and adult female apoE$^{-/-}$ (0.21 ± 0.03 mm) mice, as well as in adolescent (0.19 ± 0.04 mm) and adult (0.25 ± 0.06 mm) male WT mice (Fig. 5). Adult male apoE$^{-/-}$ mice have significantly greater periaortic fat compared to other apoE$^{-/-}$ and WT groups ($p<0.01$).

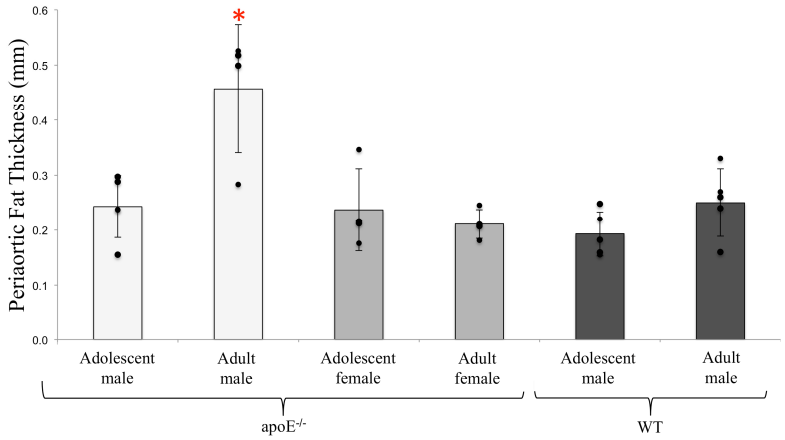

Fig. 5. Periaortic thickness values in apoE$^{-/-}$ and WT groups. Adult male apoE$^{-/-}$ mice have significantly higher periaortic thickness compared to other groups ($p<0.05$).

Biomedical Optics EXPRESS

4. Discussion

In this study we evaluated the hypothesis that PAT can be used to image and quantify periaortic fat accumulation *in vivo*. By coupling a high frequency ultrasound system and a pulsed laser, we were able to acquire images of subcutaneous and periaortic fat. We are certain that our PAT images provide lipid-specific signal for multiple reasons. We specifically utilized 1210 nm light to excite the second overtone vibrations of CH_2 bonds, which are abundantly found in lipids [5]. The *in vivo* subcutaneous fat signal also follows the geometry of the skin, while the periaortic fat signal follows the geometry of the aorta. Finally, we confirmed that our images are indeed detecting periaortic fat by performing ORO lipophilic staining on excised murine aortae (Fig. 3(F)). Our results support the application of PAT as a noninvasive *in vivo* method for preclinical studies of lipid-based conditions.

We then demonstrated the utility of this technique by detecting differences in periaortic lipid accumulation among groups of mice with different genetic background, age, and gender. Our results showed that adult male apoE$^{-/-}$ mice had significantly greater periaortic fat accumulation compared to adolescent males, female apoE$^{-/-}$, and WT mice ($p<0.01$). These results are consistent with the literature, which shows that male apoE$^{-/-}$ mice are more prone to develop cardiovascular disease compared to female apoE$^{-/-}$ mice, as they are used for aneurysm, deep vein thrombosis, and atherosclerosis studies [11–15]. In fact, male apoE$^{-/-}$ mice are more prone to developing atherosclerotic lesions especially when fed a high fat diet [11]. We also investigated if female apoE$^{-/-}$ mice fed a high fat diet would accumulate more periaortic fat compared to female mice fed a normal chow diet. In a study with separate animals, we found that there were no differences in periaortic fat thickness between mice that were placed on a high fat diet for 3 months versus normal chow (data not shown), suggesting that diet may affect luminal and periaortic fat buildup differently. While further studies are needed to explore the various mechanisms affecting luminal and periaortic fat deposition, PAT can be a powerful tool for providing noninvasive information about lipid accumulation.

While PAT has the potential to improve preclinical and clinical imaging, there still remains room to optimize this technique to improve depth of penetration and minimize photoacoustic artifacts. One limitation of our current PAT technique is that much of the 1210 nm light is absorbed by subcutaneous fat and reflected off of the skin, therefore decreasing the depth of penetration. Light attenuation by skin, muscle, and blood also limit penetration of photons to the posterior periaortic fat. As a result, we were unable to quantify lipid accumulation on the posterior aortic wall. Moreover, our current PAT setup is susceptible to artifacts that match the geometry of the skin layer and sometimes appear within a region of interest. This artifact typically appears at two times the vertical distance from the probe-skin boundary and we hypothesize that it appears due to light reflecting off of the skin surface and causing a photoacoustic effect at the probe interface. This is clearly seen in the WT images as a thick skin geometry-matching PAT signal at depths of 5 to 8 mm (Fig. 2). Imaging atherosclerotic plaques in rodents with our current PAT system is also challenging and requires further optimization for *in vivo* characterization of murine atherosclerosis. Therefore, future work will be focused on improving our system by increasing the light fluence through the skin and to employing mechanisms to minimize light reflection towards the PAT probe.

5. Conclusion

The work described here illustrates the unexplored application of PAT for preclinical *in vivo* lipid detection. While further optimization is possible, PAT has a clear advantage for rapid, noninvasive, and label-free imaging. Moreover, PAT is easily coupled with ultrasound, providing both anatomical and compositional information of tissue with better depth of penetration compared to conventional optical techniques. Development of this technology has the strong potential to lead to a myriad of applications, such as studying lipid-based disease pathology, evaluating therapeutics, and aiding in the diagnosis of human disease.

Biomedical Optics EXPRESS

Funding

Funding was provided by the American Heart Association through the Scientist Development Grant (14SDG18220010) and a Jim and Diann Robbers Research Grant to CJG.

Acknowledgments

The authors would like to thank Dr. Ji-Xin Cheng for use of the Nd:YAG OPO laser and Hannah M. Ginsberg for her assistance during animal imaging. Both Gurneet S. Sangha and Evan H. Phillips made equal contribution in the preparation of this manuscript.